Magnetic ordering and spin dynamics in potassium jarosite: A Heisenberg kagome lattice antiferromagnet

Nishiyama, M; Maegawa, S; Inami, T; Oka, Y

PHYSICAL REVIEW B **67**, 224435 (2003)

Magnetic ordering and spin dynamics in potassium jarosite: A Heisenberg kagomé lattice antiferromagnet

Masahide Nishiyama and Satoru Maegawa*
Graduate School of Human and Environmental Studies, Kyoto University, Kyoto 606-8501, Japan

Toshiya Inami
Department of Synchrotron Radiation Research, Japan Atomic Energy Research Institute, Mikazuki, Hyogo 679-5148, Japan

Yoshio Oka
Faculty of Integrated Human Studies, Kyoto University, Kyoto, 606-8501, Japan

(Received 10 October 2002; revised manuscript received 21 April 2003; published 30 June 2003)

The spin dynamics of the Heisenberg kagomé lattice antiferromagnet, potassium jarosite $KFe_3(OH)_6(SO_4)_2$, have been investigated by means of NMR. The NMR spectra confirm the long-range magnetic ordering below 65 K and the $\mathbf{q}=0$ type 120° spin structure with positive chirality in the ordered phase. Though the Heisenberg kagomé lattice antiferromagnet is considered theoretically to remain disordered down to zero temperature due to the continuous degeneracy of the ground state, the long-range magnetic ordering at the finite temperature is realized in this compound due to the weak anisotropy. The spin-lattice relaxation rate, $1/T_1$, in the ordered phase decreases sharply with lowering temperature. The experimental rate is well explained by the two-magnon process of the spin waves having an energy gap of 15 K. The temperature dependence of the sublattice magnetization also supports the existence of the spin wave. These are the first experimental evidence that the low-energy excitation in the frustrated classical kagomé lattice antiferromagnet is described by the spin wave. We calculate the spin wave in the $\mathbf{q}=0$ type 120° spin structure with weak single-ion-type anisotropy, and discuss the characteristics of the spin fluctuations in the Heisenberg kagomé lattice antiferromagnet.

DOI: 10.1103/PhysRevB.67.224435 PACS number(s): 76.60.−k, 75.40.Gb, 75.25.+z

I. INTRODUCTION

Magnetic systems which have competitive interactions even on regular lattices are called geometrically frustrated magnetic systems. These systems can not simultaneously minimize the energies of all the magnetic couplings. The antiferromagnets on the triangular lattice are a frustrated system and show interesting properties, such as the suppression of the magnetic ordering, successive phase transitions, unconventional spin structures, and large fluctuations. The kagomé lattice is also composed of triangles. While the adjacent triangles on the triangular lattice share a side, those on the kagomé lattice share only one vertex. Thus the spins on the kagomé lattice have a smaller restriction from neighboring spins than those on the triangular lattice, and the effect of the frustration on the kagomé lattice antiferromagnet is expected to be larger than that on the triangular lattice antiferromagnet. Indeed, the ideal two-dimensional Heisenberg antiferromagnet on the kagomé lattice has a continuous degeneracy in the ground state due to the ''weathervane'' rotation of the spins[1,2] and has no magnetic ordering even at zero temperature. However, small perturbations such as weak further neighboring interactions, anisotropies, and defects would resolve the degeneracy and cause the phase transition. For example, theoretically, when a weak Ising-like anisotropy is introduced into the Heisenberg kagomé antiferromagnet, the system has a magnetic transition at finite temperature and produces a peculiar spin structure having freedom of rotation around the Ising axis.[3] Moreover, it has been reported that the thermal or quantum fluctuations may resolve the degeneracy of the ground state and induce the ordering, which is called ''order by disorder.''[1,2,4] Two types of states have been discussed as candidates for the spin arrangement at zero temperature. One is the $\mathbf{q}=0$ type 120° spin alignment, and has two kinds of arrangement with plus or minus chirarities. The other type is the $\sqrt{3}\times\sqrt{3}$ type 120° spin alignment. These Neél states are shown in Fig. 1. Monte Carlo simulations suggest that the latter is favored slightly at the lowest temperature.[2] As for the spin dynamics the spin wave has been discussed theoretically,[4–6] but has not yet

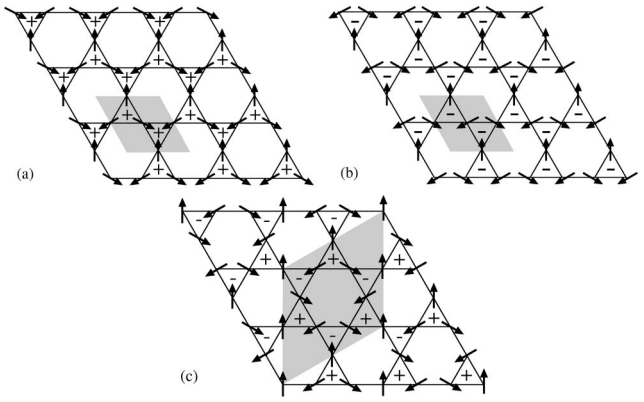

FIG. 1. Three possible Néel states of the kagomé lattice antiferromagnet: (a) $\mathbf{q}=0$ type with $+1$ chirality, (b) $\mathbf{q}=0$ type with -1 chirality, and (c) $\sqrt{3}\times\sqrt{3}$ type. Plus and minus signs indicate the chirality of spins on the elemental triangles. The shaded areas indicate the magnetic unit cells.

been observed experimentally. Unusual features such as zero energy excitations for all **k**, dispersionless mode, are expected in this system.

Despite the fascinating frustration effects and properties in kagomé lattice antiferromagnets, few experimental examples exist for the system. The jarosite family compounds, $R\mathrm{Fe}_3(\mathrm{OH})_6(\mathrm{SO}_4)_2$ and $R\mathrm{Cr}_3(\mathrm{OH})_6(\mathrm{SO}_4)_2$[$R$=K, Na, NH_4, etc.], and the magnetoplumbite isomorph, $\mathrm{SrCr}_{8-x}\mathrm{Ga}_{4+x}\mathrm{O}_{19}$, are candidates for the kagomé lattice antiferromagnets.

The compound $\mathrm{SrCr}_{8-x}\mathrm{Ga}_{4+x}\mathrm{O}_{19}$ has been studied extensively as an example of the kagomé lattice antiferromagnet. Unusual properties, such as the spin-glass-like transition and large spin fluctuations at low temperatures, have been observed.[7–9] However, this material has been found not to be an ideal kagomé antiferromagnet, because nonmagnetic Ga atoms are partially substituted at magnetic Cr sites and because the alternating kagomé and triangular planes have nonnegligible couplings.

The potassium jarosite compound, $\mathrm{KFe}_3(\mathrm{OH})_6(\mathrm{SO}_4)_2$ is a good example of a nearly two-dimensional kagomé lattice antiferromagnet. The magnetic ions Fe^{3+} with $S=5/2$ form the kagomé lattice on the c plane and are coupled antiferromagnetically with each other. Adjacent kagomé planes are separated by nonmagnetic ions, K, S, O, and H, so that the inter-plane magnetic interaction is very weak. The potassium jarosite has been investigated by neutron scattering, susceptibility, and Mëssbauer measurements.[10–13] The susceptibility indicates the occurrence of the magnetic phase transition at $T_N=65$ K. The experimental susceptibility was fitted to the high-temperature expansion calculated by Harris et al.[5], and the Weiss temperature was obtained to be $\Theta=-530$ K and the exchange interaction was estimated to be $J=23$ K.[13] Recent neutron diffraction experiment suggested that the single-ion-type anisotropy plays an important role in spin ordering.[13] On the other hand, defects have been reported to be effective in ordering, and the spin-glass-like transition occurs in hydronium jarosite.[14] Investigations concerning the microscopic magnetism and spin dynamics are desired in order to clarify the feature of the ordering, the low energy excitation, and the critical behavior. On this point of view, we performed NMR experiments for potassium jarosite, $\mathrm{KFe}_3(\mathrm{OH})_6(\mathrm{SO}_4)_2$.

The present paper is organized as follows. In Sec. II, we explain the experimental procedures. The experimental results of NMR spectrum and spin-lattice relaxation rate are presented in Sec. III. Section IV contains analyses of these experimental results and discussions on the magnetic properties of the Heisenberg kagomé lattice antiferromagnet. The magnetic structure and effects of the anisotropy are discussed based on analysis of the NMR spectra in Sec. IV A. In addition, we discuss critical behavior near the transition temperature with respect to the sublattice magnetization. In Sec. IV B, the stable spin structures for the Heisenberg kagomé antiferromagnet with the anisotropy are described theoretically, and the role of the anisotropy to the spin ordering is shown. In Sec. IV C, the spin-wave of the Heisenberg kagomé lattice antiferromagnet with the anisotropy is calculated. The dispersion relations of magnons and the spin fluctuations in the low-energy excitations are discussed. In Sec. IV D, an analysis of the spin-lattice relaxation and a discussion on the existence of the spin wave in this material are presented. The energy gap of the magnon is obtained and the values of the anisotropies are estimated. In Sec. IV E, the spin fluctuation in the paramagnetic phase is discussed. Finally, the conclusions are summarized in Sec. V. In the Appendix, the diagonalization of the spin Hamiltonian for the Heisenberg kagomé lattice antiferromagnet with the anisotropy is shown and the dispersion relations of the spin wave are obtained.

II. EXPERIMENT

The powder samples of potassium jarosite were obtained by hydrothermal synthesizing treatment. The samples were prepared by reacting $\mathrm{Fe}_2(\mathrm{SO}_4)_3$ and $\mathrm{K}_2(\mathrm{SO}_4)$ solution which was sealed in a Pyrex ampoule at 200 °C for 56 h using an autoclave. The obtained precipitation was washed using copious quantities of hot water and was then dried. The obtained samples were yellow ocher in color. The synthesis of single crystal was attempted but was not successful. The dimension of the samples was approximately 5–20 μm based on scanning electron microscope observation. The x-ray diffraction showed that the samples are single phase and that the crystal structure is hexagonal ($R\bar{3}m$) with $a=7.30$ Å and $c=17.1$ Å .

The coherent pulsed NMR method was utilized at operating frequencies between 13.1 and 276 MHz. The ^{1}H–NMR spectra were obtained by sweeping the magnetic field at fixed frequency. The spin-lattice relaxation rates for ^{1}H were obtained by measuring the spin-echo intensity as a function of the time interval between the saturation comb pulses and the two searching pulses. The protons which are observed by NMR are located in the hydroxyl groups and are in close proximity to the kagomé planes. The NMR experiments were performed in the temperature range between 1.5 and 300 K.

III. EXPERIMENTAL RESULTS

The ^{1}H–NMR spectra at 71.2 K above T_N and at 1.76 K below T_N are shown in Fig. 2. The spectrum at 71.2 K in the paramagnetic phase shows a sharp peak, whereas the spectrum in the low temperature is broad and indicates the powder pattern of the antiferromagnet. The external field H dependence of the signal intensity $I(H)$ for the powder antiferromagnets is expressed as,[15]

$$I(H)=\frac{1}{4H_A}\left|1+\frac{H_0^2-H_A^2}{H^2}\right| \tag{1}$$

for $|H_0-H_A|\leqslant H\leqslant H_0+H_A$, where H_A is the internal local field and H_0 is the resonant field for free protons. The intensity is zero for other regions of H. The broken line in Fig. 2(b) shows the calculated values under the condition that all protons experience a dipolar field H_A of identical magnitude, 4.1 kOe, from the Fe^{3+} spins. The horns at the edges of the spectrum that are deviated from the calculated line are attributed to the small amount of aligned powders induced by the

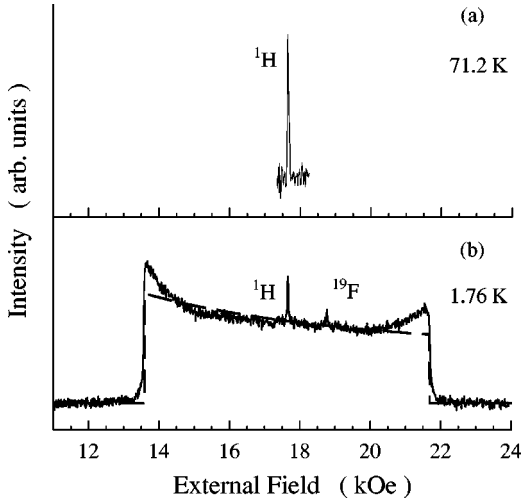

FIG. 2. ^{1}H-NMR spectra at 75.1 MHz (a) above and (b) below the transition temperature. The gray broken line in (b) indicates the calculated powder pattern of the antiferromagnet having the internal field of 4.1 kOe at proton sites. The ^{19}F signal originates from the Teflon tape around the NMR coils.

external field. The agreement between the experimental spectrum and the calculated curve indicates that there exists only one magnetic site of ^{1}H in the material.

The temperature dependence of the half width at half maximum (HWHM) of the spectra is shown in Fig. 3. The width increases sharply below 65 K, which coincides with the transition temperature. The increase in the width indicates the development of the sublattice magnetization and the long-range antiferromagnetic ordering.

The spin-lattice relaxation rate, $1/T_1$, is shown in Fig. 4. The rate shows a cusp at the transition temperature of 65 K. The rate in the paramagnetic phase is almost independent of the temperature above about 100 K and increases slightly as the temperature approaches T_N. The rate in the ordered phase decreases sharply as the temperature decreases. The frequency dependence of $1/T_1$ in both phases is weak, as shown in Figs. 5 and 6.

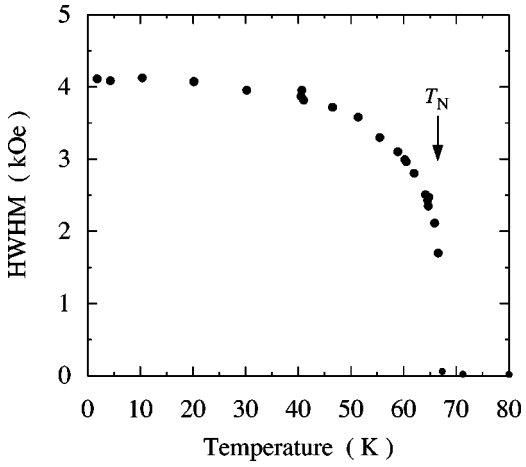

FIG. 3. Temperature dependence of the half width at half maximum of ^{1}H NMR spectra at 75.1 MHz.

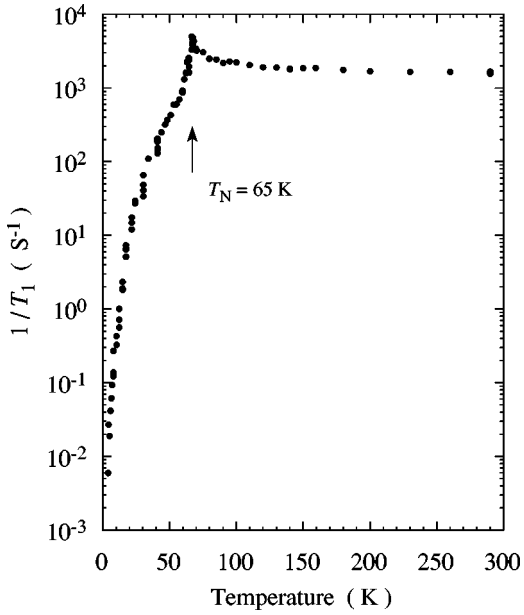

FIG. 4. Spin-lattice relaxation rate of $KFe_3(OH)_6(SO_4)_2$ at 75.1 MHz.

IV. ANALYSIS AND DISCUSSION

A. NMR spectra

In this subsection the ordered spin structure and the development of the sublattice magnetization are discussed based on the NMR spectra. The chiral vector is a significant order parameter in the Heisenberg kagomé lattice antiferromagnet. The chiral vector $\boldsymbol{\kappa}$ is defined on each triangle as

$$\boldsymbol{\kappa}=\left(\frac{2}{3\sqrt{3}}\right)(\mathbf{S}_1\times\mathbf{S}_2+\mathbf{S}_2\times\mathbf{S}_3+\mathbf{S}_3\times\mathbf{S}_1), \qquad (2)$$

where $\mathbf{S}_1$, $\mathbf{S}_2$, and $\mathbf{S}_3$ are spins on the corners of the elemental triangle. As the spins are numbered clockwise around the triangle, the chirality is $+1$ when the spins rotate clockwise

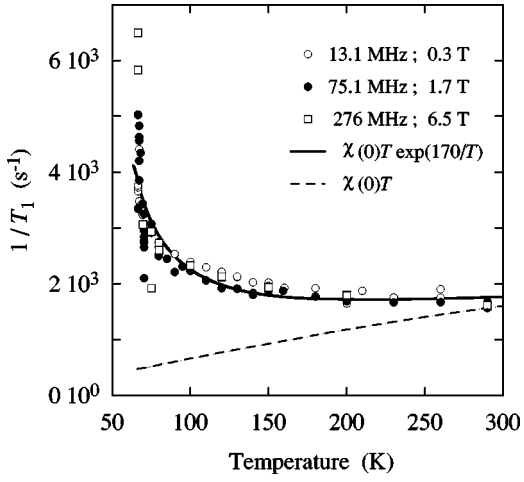

FIG. 5. Spin-lattice relaxation rate at various frequencies in the paramagnetic phase. A broken line indicates the temperature dependence of $\chi(0)T$. A solid curve indicates $1/T_1 \propto \chi(0)T\exp(170/T)$.

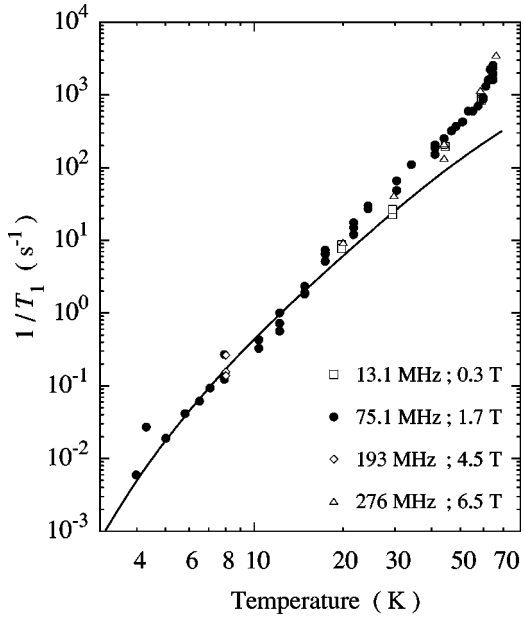

FIG. 6. Spin-lattice relaxation rate at various frequencies in the ordered phase. The solid curve shows the temperature dependence of $1/T_1$ calculated based on the two-magnon process using an energy gap of 15 K.

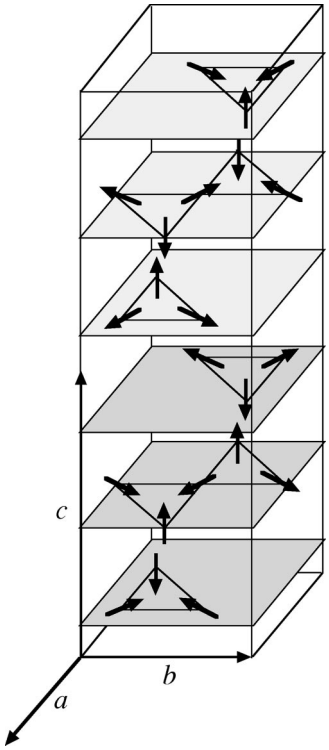

FIG. 7. Spin configuration in the ordered phase of $KFe_3(OH)_6(SO_4)_2$.

by 120° steps, and is -1 when the spins rotate counterclockwise by 120° steps. The chirality clarifies the difference between the $\mathbf{q}=0$ type configuration and the $\sqrt{3}\times\sqrt{3}$ type configuration. The $\mathbf{q}=0$ type configuration is composed of triangles having either a chirality of $+1$ or -1, while the $\sqrt{3}\times\sqrt{3}$ type configuration contains both chiralities, as shown in Fig. 1.

Since each proton is located between two irons with the same distance, the magnetic alignment composed of only $+1$ chirality produces only one kind of proton site having an identical magnitude of the dipolar field, while the alignment composed of -1 chirality produces two kinds of proton sites having different magnitudes of the fields. The NMR spectrum in the ordered phase indicates that all protons experience an internal dipolar field of identical magnitude from Fe^{3+} spins. Therefore, the ordered spin structure contains no -1 chirality, and is the $\mathbf{q}=0$ type 120° configuration with $+1$ chirality, which is shown in Fig. 1 (a).

The ^{1}H NMR spectra of OH that are nearly on the planes in $NH_4Fe_3(OH)_6(SO_4)_2$ and $NaFe_3(OH)_6(SO_4)_2$ show spectra similar to the ^{1}H spectra in $KFe_3(OH)_6(SO_4)_2$, which indicates that the magnetic structures in the ordered phase of these jarosites are identical. The spin configuration along the c axis can be discussed based on NMR spectra of the nuclei in R cations which exist between the kagomé planes. The NMR spectra of ^{1}H in NH_4 of $NH_4Fe_3(OH)_6(SO_4)_2$ and those of ^{23}Na in $NaFe_3(OH)_6(SO_4)_2$ were observed previously.[16] The NH_4 groups and Na atoms locate at the center between the triangles in the adjacent kagomé planes. The HWHM of NMR spectra for ^{1}H in NH_4 and ^{23}Na are 160 and 300 Oe in the ordered phase, respectively, which is one order of magnitude smaller than that for ^{1}H in OH groups. The small dipolar field at R sites is realized when the magnetic unit cell is twice the chemical unit cell along the c axis direction, and is identical to the chemical unit cell in the ab plane. The possible spin configuration is shown in Fig. 7. The structure is consistent with the results of the neutron diffraction experiments.[13]

Next, we discuss the development of the sublattice magnetization in the ordered phase. The HWHM increases sharply below T_N as the temperature decreases and reaches 4.1 kOe, indicating the development of the sublattice magnetization. When the sublattice magnetization M_s just below T_N is assumed to obey the power law as

$$M_s \propto \left(\frac{T_N - T}{T_N}\right)^{\beta}, \tag{3}$$

the critical exponent β is obtained to be 0.19 ± 0.01. The fitting is shown in Fig. 8. The theoretical critical exponents for several spin models are $\beta=0.253$ for $Z_2\times S_1$ ($n=2$), $\beta=0.125$ for a two-dimensional (2D) Ising system, $\beta=0.324$ for a 3D Ising system, $\beta=0.346$ for a 3D XY system and $\beta=0.365$ for a 3D Heisenberg system.[17,18] The spin model of $Z_2\times S_1$ corresponds to the frustrated XY triangular lattice antiferromagnet, whereas the other spin models are nonfrustrated systems. The experimental value for a model material of the XY triangular lattice antiferromagnet $CsMnBr_3$ is 0.25,[19] which agrees well with the predicted value.[20] The critical exponents depend on the universality class, which is determined by the symmetry of interaction, the dimensionally of the system, and the existence of frustration. As we will discuss in Sec. IV B, this compound has a

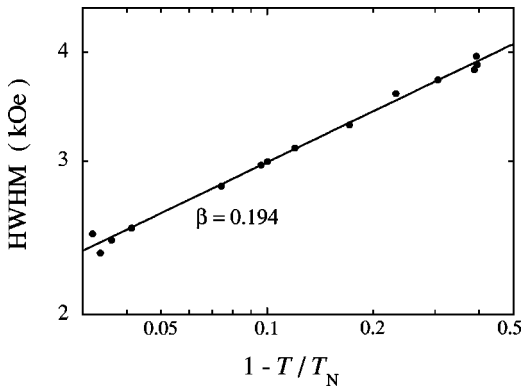

FIG. 8. Temperature dependence of half width at half maximum of ^{1}H NMR spectra at 75.1 MHz, which is plotted as a function of reduced temperature.

two-dimensional Ising symmetry due to the anisotropy. In this case the critical exponent may be expected to have a value of 0.125; however, it does not coincide with the experimental value. The Heisenberg kagomé lattice antiferromagnet, potassium jarosite, might belong to a new universality class and desires further theoretical study.

B. Stable spin structure

We now consider the conditions for the stable spin configuration that can be realized in this substance. The single-ion-type anisotropy plays a significant role in the magnetic ordering in jarosites. Each magnetic ion in the jarosite is surrounded by an octahedron composed of six oxygens. The principal axis cants about $\theta=20°$ from the c axis towards the center of the triangle and the octahedrons are distorted slightly. This surrounding of the magnetic ions would induce single-ion-type anisotropy, and the spin system can be expressed as

$$\mathcal{H}=2J\sum_{(l,m)}\mathbf{S}_l\cdot\mathbf{S}_m+D\sum_l (S_l^{y'})^2-E\sum_l [(S_l^{z'})^2-(S_l^{x'})^2], \tag{4}$$

where the local coordinate system (x',y',z') for each ion is determined by each surrounding octahedron, J is the nearest neighbor exchange interaction, and E and D are single-ion-type anisotropies with $D>0$, $E>0$, and $D,E\ll J$. The y' axis cants from the c axis with $\theta=20°$. This local coordinate system is shown in Fig. 9. Under these conditions, the spins form the umbrella configuration, in which the spins on the triangles cant slightly from the kagomé plane due to competition between the exchange interaction and the anisotropies. The canting angle from the zx plane is denoted by δ and the angle of the projection of each spin on the zx plane from the z axis is denoted by ϕ. Then, the energy of the system is given by

$$\mathcal{E}=JN[2-3\cos^2\delta]+DN[-\cos\theta\sin\delta+\sin\theta\cos\delta\cos\phi]^2 -EN[(\sin\theta\sin\delta+\cos\theta\cos\delta\cos\phi)^2-(\cos\delta\sin\phi)^2]. \tag{5}$$

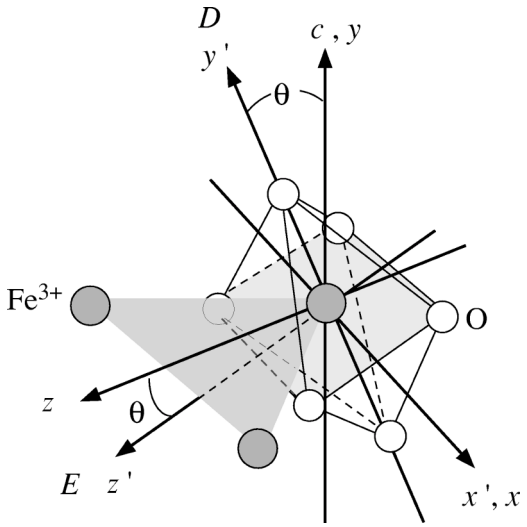

FIG. 9. Local coordinates (x,y,z) and (x',y',z') for each Fe^{3+} ion determined by each surrounding octahedron composed of oxygens. The y axis is taken to be parallel to the c axis, the z axis passes through the center of the triangle on the kagomé lattice, and the x axis lies in the kagomé plane. The y' axis is taken to be parallel to the principal axis of the octahedron and makes an angle of θ with the c axis.

The stable state with minimum energy is obtained by the variational method for the energy, with respect to δ and ϕ, as

$$\frac{\partial\mathcal{E}}{\partial\delta}=0,\quad \frac{\partial\mathcal{E}}{\partial\phi}=0. \tag{6}$$

The calculation gives three types of spin configurations having the $\mathbf{q}=0$ type 120° structure with a chirality $+1$ depending on the relations between E and D', where D' is defined as

$$D'=\frac{J}{4}\left[3+3\cos^2\theta+\frac{2D}{J} -\sqrt{\left(3+3\cos^2\theta+\frac{2D}{J}\right)^2-\frac{24D}{J}\sin^2\theta}\ \right], \tag{7}$$

and is simply described for $D\ll J$ as

$$D'\approx\frac{D\sin^2\theta}{1+\cos^2\theta+\frac{2D}{3J}}. \tag{8}$$

In the first case, when $E>D'$, the spins direct to or from the center of triangles with the canting angle δ as

$$\sin\delta=\sqrt{\frac{1}{2}-\frac{3J+(D+E)\cos2\theta}{2\sqrt{9J^2+6J(D+E)\cos2\theta+(D+E)^2}}}. \tag{9}$$

For $D,E\ll J$, δ is rewritten as

$$\sin\delta\approx\frac{D+E}{6J}\sin2\theta. \tag{10}$$

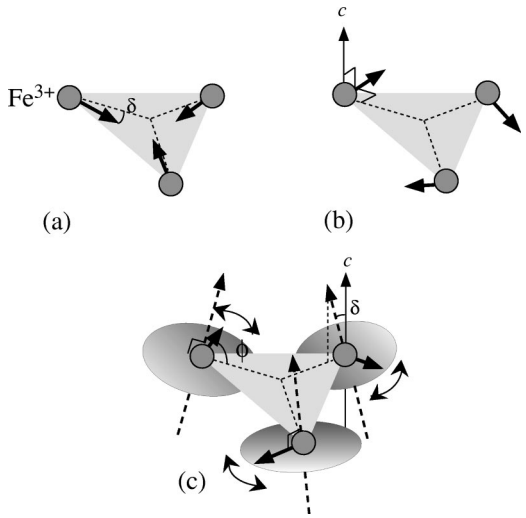

FIG. 10. Stable spin structure of (a) the first type for $E>D'$, (b) the second type for $E<D'$, and (c) the third type for $E=D'$.

This spin structure is shown in Fig. 10 (a) in the case when the spins direct to the center of the elemental triangle. The two possible spin configurations in which the spins direct either to or from the center of the triangles are equivalent with respect to energy. Second, when $E<D'$, spins are parallel or antiparallel to their own x axis. The spin structure is shown in Fig. 10 (b). Finally, when $E=D'$, each spin is in its local plane perpendicular to the axis which cants from the c axis toward the center of the triangle. In this case, the rotation of the spins in their own planes do not change the total energy, so long as the three spins form the 120° configuration. The spin structure is shown in Fig. 10 (c). The observed spin structure of the potassium jarosite is the first type, so that the condition $E>D'$ should be satisfied.

These three types of spin structures are caused by the canting of the octahedron from the c axis and the competition between the exchange interaction and the anisotropy. In the case of the first and second types, the spin structure in which the directions of all of the spins are inverted has the same energy as that of the original structure. Therefore, the spin system is regarded as a two-dimensional Ising system, which would have a magnetic transition at finite temperature. The two-dimensional ordering in the planes would simultaneously induce the three-dimensional ordering, when there exists at least nonzero interplane interactions. The magnetic ordering at finite temperature and the spin structure in the potassium jarosite are found to be dominated by the anisotropy.

C. Spin wave in the Heisenberg kagomé antiferromagnet with small anisotropy

The dispersion relation for the isotropic Heisenberg kagomé lattice antiferromagnet having a $\mathbf{q}=0$ type spin structure was calculated by Harris *etal.*[5] and Asakawa *etal.*[6] We extended their methods for the system of jarosite by introducing the single-ion-type anisotropies. The Hamiltonian is rewritten in terms of the sublattices as

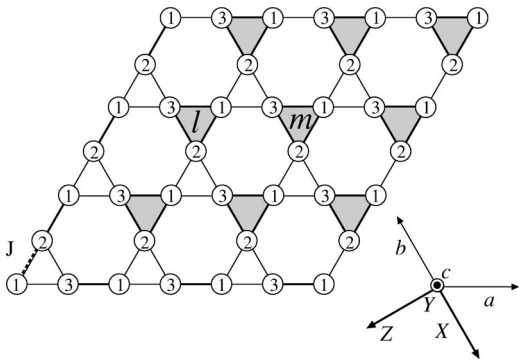

FIG. 11. Sublattices of the $\mathbf{q}=0$ structure on the kagomé lattice. l and m indicate the triangles. The numbers 1, 2, and 3 indicate three sublattices. The axes **a**, **b**, and **c** are the crystallographic axes of the trigonal. The coordinate system (X,Y,Z) is the crystal frame. The X axis is antiparallel to the b axis, and the Z axis is parallel to $-2\mathbf{a}-\mathbf{b}$.

$$\mathcal{H}=J\sum_{l,\alpha}\sum_{m,\beta}\mathbf{S}_{l,\alpha}\cdot\mathbf{S}_{m,\beta}+D\sum_{l,\alpha}(S^{y'}_{l,\alpha})^2$$

$$-E\sum_{l,\alpha}\{(S^{z'}_{l,\alpha})^2-(S^{x'}_{l,\alpha})^2\}, \tag{11}$$

where l and m denote the elemental triangles, and α and β indicate the sublattices, $\alpha,\beta=1,2,3$ for $\mathbf{q}=0$ spin structure. These configurations are illustrated in Fig. 11. The summation on sites (l,α) and (m,β) in Eq. (11) are restricted to be over the nearest neighbors. The single-ion-type anisotropies D and E are assumed to be $D>0$, $E>0$, and $D,E\ll J$. In this case, the cant angle δ is negligible, spins lie on the kagomé plane, and D' is expressed as $D\sin^2\theta/(1+\cos^2\theta)$. The local coordinate systems (x,y,z) and (x',y',z') are identical to those in Sec. IV B, and have been shown in Figs. 9 and 11. The stable direction of each spin is along the z axis, and so the directions of spins on the 1, 2, and 3 sublattices have angles of 0°, 120°, and −120° from the Z axis in the ZX plane, respectively.

The spins in the crystal frame (X,Y,Z) are written by the spin components in the local coordinate system (x,y,z) as

$$\mathbf{S}_{l,\alpha}=\begin{pmatrix}S^X_{l,\alpha}\\S^Y_{l,\alpha}\\S^Z_{l,\alpha}\end{pmatrix}=\begin{pmatrix}S^x_{l,\alpha}\cos\dfrac{2\pi(\alpha-1)}{3}-S^z_{l,\alpha}\sin\dfrac{2\pi(\alpha-1)}{3}\\S^y_{l,\alpha}\\S^x_{l,\alpha}\sin\dfrac{2\pi(\alpha-1)}{3}+S^z_{l,\alpha}\cos\dfrac{2\pi(\alpha-1)}{3}\end{pmatrix}. \tag{12}$$

In addition, the spins in the inclined local coordinate system (x',y',z') are related to the local coordinate system (x,y,z) as

$$\begin{pmatrix}S^{x'}_{l,\alpha}\\S^{y'}_{l,\alpha}\\S^{z'}_{l,\alpha}\end{pmatrix}=\begin{pmatrix}S^x_{l,\alpha}\\S^y_{l,\alpha}\cos\theta+S^y_{l,\alpha}\sin\theta\\-S^y_{l,\alpha}\sin\theta+S^z_{l,\alpha}\cos\theta\end{pmatrix}. \tag{13}$$

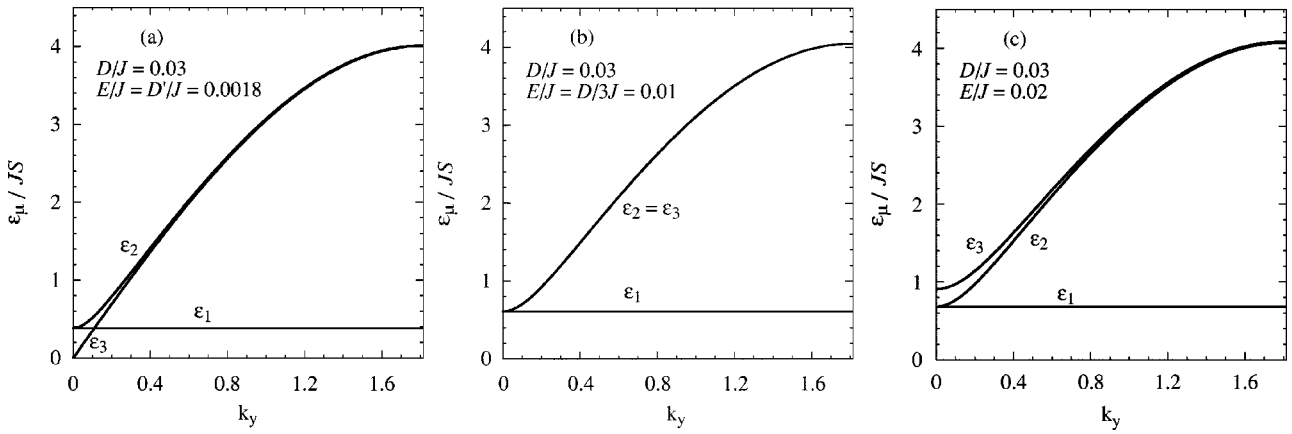

FIG. 12. Dispersion relations for various values of anisotropies.

Then, the Hamiltonian [Eq. (11)] is transformed to

$$\mathcal{H}=\mathcal{H}_J+\mathcal{H}_D+\mathcal{H}_E, \tag{14}$$

with

$$\mathcal{H}_J=J\sum_{l,\alpha}\sum_{m,\beta}\left[-\frac{1}{2}S^x_{l,\alpha}S^x_{m,\beta}+S^y_{l,\alpha}S^y_{m,\beta}-\frac{1}{2}S^z_{l,\alpha}S^z_{m,\beta}\right.$$
$$\left.-(S^x_{l,\alpha}S^z_{m,\beta}-S^z_{l,\alpha}S^x_{m,\beta})\sin\frac{2\pi(\beta-\alpha)}{3}\right], \tag{15a}$$

$$\mathcal{H}_D=D\sum_{l,\alpha}(S^z_{l,\alpha}\sin\theta+S^y_{l,\alpha}\cos\theta)^2, \tag{15b}$$

$$\mathcal{H}_E=E\sum_{l,\alpha}[(S^x_{l,\alpha})^2-(S^z_{l,\alpha}\cos\theta-S^y_{l,\alpha}\sin\theta)^2]. \tag{15c}$$

The diagonalization of the Hamiltonian [Eq. (14)] is shown in the Appendix. The obtained dispersion relations of magnons in the case of $|\mathbf{k}|\ll 1$ and $D,E\ll J$ are described as

$$\epsilon_1(\mathbf{k})\approx 2S\sqrt{3J(D+E)(2\cos^2\theta-1)}=\Delta\epsilon_1, \tag{16a}$$

$$\epsilon_2(\mathbf{k})\approx\sqrt{\Delta\epsilon_1^2+12J^2S^2\ \mathbf{k}^2}, \tag{16b}$$

$$\epsilon_3(\mathbf{k})\approx\sqrt{\Delta\epsilon_3^2+12J^2S^2\ \mathbf{k}^2}, \tag{16c}$$

where

$$\Delta\epsilon_3\approx 2S\sqrt{6J[E(1+\cos^2\theta)-D\sin^2\theta]}. \tag{17}$$

Characteristic examples of dispersion relations are shown in Figs. 12(a), 12(b), and 12(c), where $D/J=0.03$. In case (a), $E/J=D'/J=0.0018$, in case (b), $E/J=D/3J=0.01$, and in case (c), $E/J=0.02$. The cant angle θ is 20° for the real jarosite and $D'=0.062D$. The dispersion relations have energy gaps due to the anisotropies. The dispersion relation $\epsilon_1(\mathbf{k})$ is the dispersionless flat mode, while the dispersion has a slope when the next nearest neighbor interaction is introduced. The gap energy $\Delta\epsilon_3$ vanishes when $E=D'$, as shown in Fig. 12(a). For $E<D'$, $\Delta\epsilon_3$ is complex, and this condition agrees with the unstable condition for the first type spin structure, which is discussed in the previous subsection. The energy ϵ_3 is smaller than ϵ_2 when $D'<E<D/3$. When $E=D/3$, ϵ_2 is equal to ϵ_3, as shown in Fig. 12(b). When $E>D/3$, ϵ_3 is larger than ϵ_2, as shown in Fig. 12(c).

There exist three types of low-energy excitation modes in the ordered triangular spin structure,[21,22] which correspond to the rotational fluctuations around the three axes, as are shown in Fig. 13. These excitation modes correspond to the dispersion relations $\epsilon_\mu(\mathbf{k})$ of magnons for the $\mathbf{q}=0$ type spin structure on the kagomé lattice antiferromagnet, as shown in the following. When we consider the case for $\theta=0°$ and $D,E\ll J$, for simplicity, the gap energies are given by

$$\Delta\epsilon_1^0=\Delta\epsilon_2^0\approx 2S\sqrt{3J(D+E)}, \tag{18a}$$

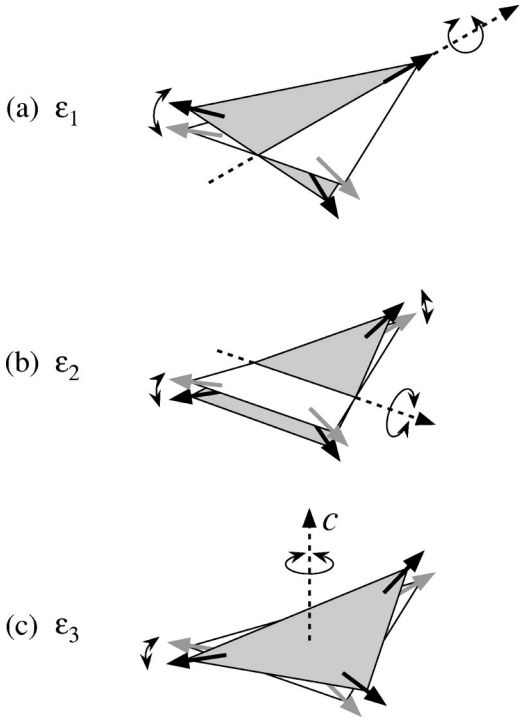

FIG. 13. Low-energy excitation modes of the triangular spin structure. These modes correspond to the swinging motions around the broken lines.

$$\Delta\epsilon_3^0 \approx 2S\sqrt{12JE}. \tag{18b}$$

The gap energy $\Delta\epsilon_3^0$ depends only on E, whereas $\Delta\epsilon_1^0$ and $\Delta\epsilon_2^0$ both depend on E and D. Thus, the low-energy excitation mode of ϵ_3 is found to be fluctuation occurring primarily in the spin plane, as shown in Fig. 13(c). The flat mode, which is localized for the spins on the hexagons, is realized by the connection of the fluctuation which is shown in Fig. 13(a). The remaining ϵ_2 corresponds to the excitation shown in Fig. 13(b).

D. Spin-lattice relaxation rate in the ordered phase

The experimental data of the relaxation rate in the ordered phase is strongly dependent on temperature. This temperature dependence of the relaxation rate $1/T_1$ is explained by the two-magnon process of the spin wave in the Heisenberg kagomé lattice antiferromagnet with the single-ion-type anisotropies. The relaxation rate due to the two-magnon process was investigated by Moriya,[23] and was extended to the case of the triangular lattice antiferromagnet by Maegawa.[24] We herein apply their calculations to the case of the kagomé lattice.

The fluctuation of the electron spin $\mathbf{S}_i$ at the i site is described by

$$\delta\mathbf{S}_i = \mathbf{S}_i - \langle \mathbf{S}_i \rangle. \tag{19}$$

The fluctuation of spins causes the fluctuation of local fields at nuclear sites through dipolar interaction. The nuclear spin-lattice relaxation rate is given by[23]

$$\frac{1}{T_1} = \gamma_e^2\gamma_n^2\hbar^2 \sum_i \sum_j \frac{1}{R_i^3}\frac{1}{R_j^3} \times \left\{ F_{ij}\int_{\infty}^{-\infty} dt \cos\omega_n t \langle \delta S_i^Z(t)\delta S_j^Z(0)\rangle + \frac{1}{4}F'_{ij}\int_{\infty}^{-\infty} dt \cos\omega_n t [\langle \delta S_i^+(t)\delta S_j^-(0)\rangle + \langle \delta S_i^-(t)\delta S_j^+(0)\rangle] \right\}, \tag{20}$$

where $\delta S_i^{\pm} = \delta S_i^X \pm \delta S_i^Y$. F_{ij} and F'_{ij} are geometrical factors derived from the dipolar interaction. ω_n is the nuclear Zeeman frequency, and γ_e and γ_n are the electric and nuclear gyromagnetic ratios, respectively. The spin correlation functions in Eq. (20) are rewritten by the small deviations $(\delta S_i^x, \delta S_i^y, \delta S_i^z)$ using Eqs. (12) and (13). These deviations are described by the spin wave operators using the Holstein-Primakoff method. Precise calculations reveal that the correlation function $\langle \delta S_i^Z(t)\delta S_j^Z(0)\rangle$ yields the dominant contribution to the relaxation due to the two-magnon process. This implies that only the fluctuation in the ZX plane contributes to the relaxation rate.

The rate $1/T_1$ due to the two-magnon process is expressed as[23,24]

$$\frac{1}{T_1} = \frac{\pi}{2}\gamma_e^2\gamma_n^2\hbar^2 \sum_{i,j} G_{ij}\int_{\omega_0}^{\omega_m}\left\{1+\left(\frac{\omega_m}{\omega}\right)^2\right\} \times \frac{e^{\hbar\omega/k_BT}}{(e^{\hbar\omega/k_BT}-1)^2} N(\omega)^2 d\omega, \tag{21}$$

where G_{ij} is the geometrical factor transformed from F_{ij} and F'_{ij}, ω_m is the maximum frequency, ω_0 is the energy gap and $N(\omega)$ is the state density of magnons. When the long wave approximation is applied for the dispersion relation, the relaxation rate is given by[24]

$$\frac{1}{T_1} = \frac{9\pi\gamma_e^2\gamma_n^2\hbar^3}{2k_B}\frac{T^5}{(T_m^2 - T_0^2)^3}\sum_{i,j} G_{ij}\int_{T_0/T}^{T_m/T}\frac{e^x}{(e^x-1)^2} \times \left\{x^2 - \left(\frac{T_0}{T}\right)^2\right\}\left\{x^2 + \left(\frac{T_m}{T}\right)^2\right\} dx, \tag{22}$$

where $T_m = \hbar\omega_m/k_B$ and $T_0 = \hbar\omega_0/k_B$. The temperature dependence of $1/T_1$ calculated using $T_0 = 15$ K and $T_m = 4SJ = 230$ K is shown by the solid curve in Fig. 6. The exchange energy J is 23 K, which has been derived from the experimental susceptibility. The fitting parameters are the gap energy T_0 and the prefactor. The agreement between the experimental data and the calculated values is good over the three order of the magnitude in the low temperature region.

As discussed above, only the fluctuation in the ZX plane contributes to the relaxation in the two-magnon process. The mode $\epsilon_3(\mathbf{k})$ corresponds to the fluctuation in the ZX plane and is almost independent of the external field. This coincides with the experimental data, which indicate that the relaxation rate in the ordered phase is independent on the external field. The values of E and D are estimated from the experimental energy gap of 15 K, $E > D'$ and Eq. (17) as

$$0.037 < E < 1.46, \tag{23a}$$

$$D = 16.1E - 0.56, \tag{23b}$$

where E and D are in K.

We show, moreover, that the temperature dependence of the sublattice magnetization $M_s(T)$ at low temperatures is also explained by the spin wave. The reduction of the sublattice magnetization from the saturated value due to the spin wave excitations is expressed as

$$M_s(0) - M_s(T) = NS\mu_B \sum_{\mathbf{k}} \frac{1}{e^{\hbar\omega_k/k_BT}-1}. \tag{24}$$

Applying the long wave approximation on the dispersion relation, the temperature dependence of the reduction at low temperatures is given by

$$M_s(0) - M_s(T) \propto T^2 \int_{T_0/T}^{T_m/T} \frac{x}{e^x - 1} dx. \tag{25}$$

The values calculated using $T_0 = 15$ K and $T_m = 230$ K are shown by the solid curve in Fig. 14. The agreement between

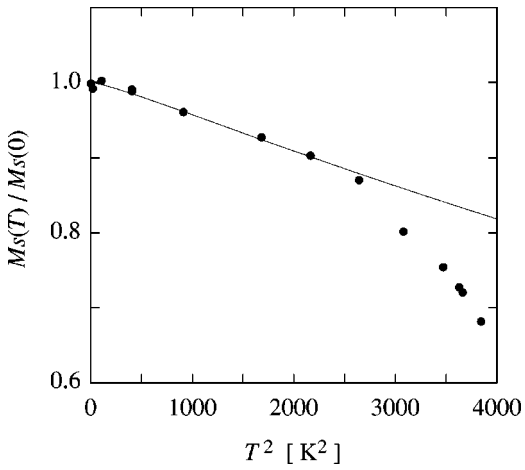

FIG. 14. Sublattice magnetization of $KFe_3(OH)_6(SO_4)_2$. The solid curve shows the temperature dependence of the sublattice magnetization due to the spin wave.

the calculated value and the magnetization derived from the NMR spectrum width is good and supports the existence of the spin wave in this system.

Finally, we briefly mention the origin of the anisotropy. The obtained spin structure and energy gap of the magnon dispersion clearly demonstrate the existence of the anisotropy. The single-ion-type anisotropies are produced due to the spin-orbit interaction and are expressed by the second-order perturbation between the ground state and the excited state in a crystal field. So the single-ion-type anisotropies can exist in jarosites, though the orbital moments of Fe^{3+} ions are zero in the $3d^5\ ^6S$ ground state. Recently it, was proposed that the magnetic ordering in jarosites can be induced by the anisotropy of Dzyaloshinsky–Moriya interaction, which is also derived by the second-order perturbation of the spin-orbit interaction.[25] The existence of anisotropy is clear, however, further investigation is needed to specify the origin of the anisotropy.

E. Spin-lattice relaxation rate in paramagnetic phase

In the paramagnetic phase the fluctuation of the field at ^1H sites is caused by the paramagnetic fluctuation of Fe^{3+} spins. The nuclear spin-lattice relaxation rate $1/T_1$ is given by[26,27]

$$\frac{1}{T_1}=\frac{(\hbar\gamma_e\gamma_n)^2}{4\pi}\int_{-\pi}^{\pi}d\mathbf{q}\int_{-\infty}^{\infty}dt\cos\omega_n t[A^+(\mathbf{q})\times\langle\{S^+_{\mathbf{q}}(t)S^-_{-\mathbf{q}}(0)\}\rangle+A^Z(\mathbf{q})\langle\{S^Z_{\mathbf{q}}(t)S^Z_{-\mathbf{q}}(0)\}\rangle], \tag{26}$$

where $A^\xi(\mathbf{q})$ is the geometrical coefficient, ξ is $+$ or Z, and $\mathbf{q}$ is the wave vector in the first Brillouin zone. Based on the fluctuation dissipation theorem and the high temperature approximation, $1/T_1$ in the paramagnetic phase is rewritten as[24]

$$\frac{1}{T_1}=\frac{\gamma_e^2}{4\pi}k_BT\int_{-\pi}^{\pi}d\mathbf{q}\times\left[A^+(\mathbf{q})\chi^+(\mathbf{q})\frac{2\Gamma^+_{\mathbf{q}}}{\omega_e^2+\Gamma^{+2}_{\mathbf{q}}}+A^Z(\mathbf{q})\chi^Z(\mathbf{q})\frac{2}{\Gamma^Z_{\mathbf{q}}}\right], \tag{27}$$

where $\Gamma^\xi_{\mathbf{q}}$ is a damping constant of the spin correlations and $\chi^\xi(\mathbf{q})$ is the susceptibility. Since the experimental data of the relaxation rates are independent of NMR frequencies, either the second term in the integral of Eq. (27) is dominant or $\omega_e \ll \Gamma^+_{\mathbf{q}}$ in the first term is satisfied. When $\Gamma^\xi_{\mathbf{q}}$ and $\chi^\xi(\mathbf{q})$ are assumed to be $\mathbf{q}$ independent and isotropic at high temperatures, the rate is simply expressed as

$$\frac{1}{T_1}\propto\chi(0)\ \frac{T}{\Gamma}, \tag{28}$$

where $\chi(0)$ is the static susceptibility. This formula, having the temperature independent Γ, agrees very well with the experimental results for the relaxation rate in the triangular lattice antiferromagnet $CsNiBr_3$.[24] For the jarosite the calculated temperature dependence of the rate using the measured susceptibility and a constant Γ is shown by a broken line in Fig. 5. The calculated curve does not fit the experimental data well. The susceptibility data show the development of the short range correlation in this temperature region. The disagreement may be attributed to the development of the short-range spin correlation.

When Γ is assumed to be temperature dependent as

$$\Gamma\propto\exp\left(-\frac{\Delta}{T}\right), \tag{29}$$

the temperature dependence of the relaxation rate is given by

$$\frac{1}{T_1}\propto\chi(0)T\exp\left(\frac{\Delta}{T}\right). \tag{30}$$

The calculated curve using $\Delta=170$ K is shown by a solid curve in Fig. 5. This curve fits the experimental data well, except for the temperature region in the vicinity of the transition. However, the reason why the damping obeys the activation type in the paramagnetic phase remains unclear. In addition to the temperature dependence of $\Gamma_{\mathbf{q}}$ related to the time correlation of spins, the $\mathbf{q}$ dependence of $\chi(\mathbf{q})$ related to the spatial correlation may have to be considered.

The divergent behavior of $1/T_1$ near T_N is attributed to the effect of the critical phenomenon, and the temperature dependence of $1/T_1$ may yield the dynamical critical exponents. However, since the signal intensities become very small and $1/T_1$ data were scattered near the transition temperature, the exponents cannot be determined.

V. CONCLUSION

The jarosite family compounds, $RFe_3(OH)_6(SO_4)_2$ [R = K, NH_4, Na, Rb], are examples of the classical Heisenberg kagomé lattice antiferromagnet. Fe^{3+} ions form a

kagomé lattice in the c plane and couple antiferromagnetically with nearest neighbors. Potassium jarosite $KFe_3(OH)_6(SO_4)_2$ has been investigated by ^{1}H-NMR measurements.

NMR spectra show the long-range magnetic ordering below $T_N = 65$ K. The spectra show a narrow peak in the paramagnetic region, with a half width of 10 Oe, and become broader in the ordered phase up to 4.1 kOe at the lowest temperature. The broad spectra in the ordered phase show the pattern for the powdered antiferromagnets, and indicate that the ^{1}H sites are magnetically unique and that the magnetic structure in the ordered phase is the $\mathbf{q}=0$ type 120° spin structure with chirality $+1$. Possible magnetic structures due to the anisotropy are analyzed by the variational method and the magnetic structure of the jarosite is shown to be stabilized by the weak single-ion-type anisotropy due to the local symmetry at Fe sites in the crystal.

The spin-lattice relaxation rate $1/T_1$ in the ordered phase decreases sharply with decreasing temperature, and is well explained by the two-magnon process with the energy gap of the magnon dispersion. A spin wave analysis has been performed on the $\mathbf{q}=0$ type 120° spin structure with a chirality $+1$ of the kagomé lattice Heisenberg antiferromagnet with weak single-ion-type anisotropy. Three dispersion relations are obtained and have energy gaps caused by the anisotropy. The experimental data of $1/T_1$ in the ordered phase agree fairly well with the values calculated for the energy gap of 15 K. Then the values of the anisotropy are estimated. The temperature dependence of the sublattice magnetization also supports the existence of the spin wave. In the paramagnetic phase $1/T_1$ increases slowly as the temperature decreases, and diverges as the temperature approaches T_N. The relaxation rate is analyzed in terms of the paramagnetic fluctuation on the antiferromagnet. Studies concerning the temperature dependence of the damping factor and the q dependence of the susceptibility are desired for a precise analysis.

ACKNOWLEDGMENTS

The authors would like to thank Professor S. Miyashita for valuable discussions, Dr. A. Oyamada for helpful experimental advice, and N. Tanaka for his collaboration during the initial stage of the experiments.

APPENDIX: DIAGONALIZATION OF THE HAMILTONIAN FOR SPIN WAVE

Here we show the calculation of the diagonalization of the Hamiltonian equation (14) and get the dispersion relations. Following the Holstein-Primakoff method the spins are expressed by the annihilation and creation operators as

$$S^x_{l,\alpha} = \sqrt{\frac{S}{2}}[c^\dagger_{l,\alpha} + c_{l,\alpha}], \tag{A1a}$$

$$S^y_{l,\alpha} = i\sqrt{\frac{S}{2}}[c^\dagger_{l,\alpha} - c_{l,\alpha}], \tag{A1b}$$

$$S^z_{l,\alpha} = S - c^\dagger_{l,\alpha} c_{l,\alpha}. \tag{A1c}$$

The operators are transformed as

$$c_{l,\alpha} = \frac{1}{\sqrt{N}} \sum_{\mathbf{k}} c_\alpha(\mathbf{k}) e^{i\mathbf{k}\cdot(\mathbf{r}_l + \mathbf{r}_\alpha)}. \tag{A2}$$

The Hamiltonian [Eq. (14)] is transformed to

$$\begin{aligned}\mathcal{H} = &-3NS^2(2J + E\cos^2\theta - D\sin^2\theta) + S\sum_{\mathbf{k},\alpha,\beta}\Big\{[(4J \\ &+ 3E\cos^2\theta - 3D\sin^2\theta + D)\delta_{\alpha\beta} + J\Lambda_{\alpha\beta}]c^\dagger_\alpha(\mathbf{k})c_\beta(\mathbf{k}) \\ &+ \left[\frac{1}{2}(E + E\sin^2\theta - D\cos^2\theta)\delta_{\alpha\beta} - \frac{3}{2}J\Lambda_{\alpha\beta}\right] \\ &\times[c^\dagger_\alpha(\mathbf{k})c^\dagger_\beta(-\mathbf{k}) + c_\alpha(\mathbf{k})c_\beta(-\mathbf{k})]\Big\},\end{aligned} \tag{A3}$$

where N is the number of unit cells, and $q_1 = k_x$, $q_2 = (k_x - \sqrt{3}k_y)/2$, $q_3 = q_1 - q_2$, and $\Lambda_{\alpha\beta}$ are the elements of the matrix Λ,

$$\Lambda = \begin{pmatrix} 0 & \cos q_3 & \cos q_1 \\ \cos q_3 & 0 & \cos q_2 \\ \cos q_1 & \cos q_2 & 0 \end{pmatrix}. \tag{A4}$$

Using the Bogoliubov transformation, the Hamiltonian $\mathcal{H}$ is diagonalized as

$$\begin{aligned}\mathcal{H} = &-3NS(S+1)(2J + E\cos^2\theta - D\sin^2\theta) \\ &+ \sum_{\mathbf{k}} \epsilon_\mu(\mathbf{k})\left[a^\dagger_\mu(\mathbf{k})a_\mu(\mathbf{k}) + \frac{1}{2}\right].\end{aligned} \tag{A5}$$

$\epsilon_\mu(\mathbf{k})$ is the energy of magnons given by

$$\begin{aligned}\epsilon_\mu(\mathbf{k}) = &2S\sqrt{J(2 - \lambda_\mu(\mathbf{k})) + (E - D) + (E + D)\cos^2\theta} \\ &\times\sqrt{2J(1 + \lambda_\mu(\mathbf{k})) + (D + E)(2\cos^2\theta - 1)},\end{aligned} \tag{A6}$$

where μ indicates mode 1, 2, or 3 and λ_μ is the eigenvalue of the matrix Λ, as follows:

$$\lambda_1 = -1, \tag{A7a}$$

$$\lambda_{2,3} = \tfrac{1}{2} \mp \sqrt{\cos^2 q_1 + \cos^2 q_2 + \cos^2 q_3 - \tfrac{3}{4}}. \tag{A7b}$$

In the case of $|\mathbf{k}| \ll 1$, and $D, E \ll J$, the magnon energy is expressed as

$$\epsilon_1(\mathbf{k}) \approx 2S\sqrt{3J(D+E)(2\cos^2\theta - 1)} = \Delta\epsilon_1, \tag{A8a}$$

$$\epsilon_2(\mathbf{k}) \approx \sqrt{\Delta\epsilon_1^2 + 12J^2S^2\ \mathbf{k}^2}, \tag{A8b}$$

$$\epsilon_3(\mathbf{k}) \approx \sqrt{\Delta\epsilon_3^2 + 12J^2S^2\ \mathbf{k}^2}, \tag{A8c}$$

where

$$\Delta\epsilon_3 \approx 2S\sqrt{6J[E(1 + \cos^2\theta) - D\sin^2\theta]}. \tag{A9}$$

*Email address: d54355@sakura.kudpc.kyoto-u.ac.jp

[1] I. Ritchey, P. Chandra, and P. Coleman, Phys. Rev. B **47**, 15 342 (1993).
[2] J. N. Reimers and A. J. Berlinsky, Phys. Rev. B **48**, 9539 (1993).
[3] A. Kuroda and S. Miyashita, J. Phys. Soc. Jpn. **64**, 4509 (1995).
[4] A. Chubukov, Phys. Rev. Lett. **69**, 832 (1992).
[5] A. B. Harris, C. Kallin, and A. J. Berlinsky, Phys. Rev. B **45**, 2899 (1992).
[6] H. Asakawa and M. Suzuki, Physica A **205**, 687 (1994).
[7] G. Aeppli, C. Broholm, A. Ramirez, G. P. Espinosa, and A. S. Cooper, J. Magn. Magn. Mater. **90&91**, 255 (1990).
[8] C. Broholm, G. Aeppli, G. P. Espinosa, and A. S. Cooper, Phys. Rev. Lett. **65**, 3173 (1990).
[9] Y. J. Uemura, A. Keren, K. Kojima, L. P. Le, G. M. Luke, W. D. Wu, Y. Ajiro, T. Asano, Y. Kuriyama, M. Mekata, H. Kikuchi, and K. Kakurai, Phys. Rev. Lett. **73**, 3306 (1994).
[10] M. G. Townsend, G. Longworth, and E. Roudaut, Phys. Rev. B **33**, 4919 (1986).
[11] M. Takano, T. Shinjo, and T. Takada, J. Phys. Soc. Jpn. **30**, 1049 (1971).
[12] S. Maegawa, M. Nishiyama, N. Tanaka, A. Oyamada, and M. Takano, J. Phys. Soc. Jpn. **65**, 2776 (1996).
[13] T. Inami, M. Nishiyama, S. Maegawa, and Y. Oka, Phys. Rev. B **61**, 12 181 (2000).
[14] A. S. Wills, A. Harrison, C. Ritter, and R. I. Smith, Phys. Rev. B **61**, 6156 (2000).
[15] Y. Yamada and A. Sakata, J. Phys. Soc. Jpn. **55**, 1751 (1986).
[16] M. Nishiyama, N. Tanaka, S. Maegawa, A. Oyamada, and M. Takano, Czech. J. Phys. **46**, 2053 (1996).
[17] H. Kawamura, J. Phys. Soc. Jpn. **61**, 1299 (1992).
[18] H. Kawamura and S. Miyashita, J. Phys. Soc. Jpn. **53**, 4138 (1984).
[19] Y. Ajiro, T. Nakashima, Y. Unno, H. Kadowaki, M. Mekata, and N. Achiwa, J. Phys. Soc. Jpn. **57**, 2648 (1988).
[20] T. E. Mason, B. D. Gaulin, and M. F. Collins, Phys. Rev. B **39**, 586 (1989).
[21] T. Suzuki and Y. Natsume, J. Phys. Soc. Jpn. **56**, 1577 (1987).
[22] H. Tanaka, S. Teraoka, E. Kakehashi, K. Iio, and K. Nagata, J. Phys. Soc. Jpn. **57**, 3979 (1988).
[23] T. Moriya, Prog. Theor. Phys. **16**, 23 (1956).
[24] S. Maegawa, Phys. Rev. B **51**, 15 979 (1995).
[25] M. Elhajal, B. Canals, and C. Lacroix, Phys. Rev. B **66**, 14 422 (2002).
[26] T. Moriya, Prog. Theor. Phys. **28**, 371 (1962).
[27] D. Hone, C. Scherer, and F. Borsa, Phys. Rev. B **9**, 965 (1974).